Supplementary Materials for

Unlocking coherent control of ultrafast plasmonic interaction

Authors: Eyal Bahar, Uri Arieli, Maayan Vizner Stern, Haim Suchowski

Correspondence to: eyalb@tauex.tau.ac.il

Section S1. Experimental set-up

Dynamical coherent control over extreme ultrafast interactions is unquestionably very challenging as it requires control over extremely ultrashort timescales. In the spectral domain, the challenge translates to precise and delicate manipulation of the spectral phase function of the driving pulse over a sizable bandwidth, as dictated by Fourier transform. In such systems, delicate dispersion management is essential since even the dispersion induced by the propagation in air significantly hinders the fidelity and temporal resolution extreme ultrafast processes demand, such as plasmonic excitations. Furthermore, any conventional strong focusing elements, commonly used in nano-optical systems, such as high NA immersion objective lens', further complicates the spectral shape of the pulse as they are immensely dispersive as well as contribute considerably to high order terms in the spectral phase. These obstacles in coherent control application are typically addressed by utilizing the pulse shaper itself as a compensation mask. However, such implementations substantially lower fidelity of the applied spectral mask, restricting the resolution and accuracy of the spatial light modulator (SLM). As a result, these impede controllability, narrowing the coherent control landscape and inhibiting the realization of control over ultrafast processes within the excitation lifetimes. To address these challenges, which are critically required for extreme ultrashort plasmonic lifetimes, allowing for our SLM to solely be used as an active dynamical coherent control device, we carefully designed a dispersionless pulse shaper set up, effectively freeing the SLM from dispersion management (illustrated in Figure 1). Our set up consists of a carefully constructed mirror-based (parabolic mirror, f = 500 mm) 4f pulse shaper (Plane Ruled reflective grating, 1200 G/mm Newport, Richardson) SLM, (Jenoptik 640d) accompanied by a custom-made chirped mirror set-up (Laser

Quantum), tunable CaF2 ultrafast wedge pair followed by a mirror-based objective lenses (Edmund optics, infinity corrected 15X NA 0.28 and (Thorlabs, LMM-15X-UVV, infinity corrected 15X, 0.30 NA). The beam was maximally focused to a diameter of ~10 micrometers at FWHM. The linear spectrum of the laser as well as the nonlinear signals produced in experiment were collected by a Isoplane320 spectrometer equipped with a PIXIS camera.

Nanostructures fabrication processes

Nanostructures were fabricated on an ITO covered glass (Sigma Aldrich). The samples were first covered with PMMA-A4 polymer and spin-coated for one minute at 7,000 RPM. The electron beam (Raith150) used was a 10 kV beam, aperture 6 mm WD, and a dose was deposited in single-pixel lines. Samples were then developed in MIBK/IPA (1:3) for 1 min and rinsed in isopropanol for 20 s. A concentration of 40 nm of gold was then evaporated on the sample with an E-Beam Evaporator (VST evaporator). Lift-off was performed with acetone and followed with a final wash in isopropanol. Nanostructure arrays of 50x50 micrometer. In each array the nanostructured were to design to have equal effective length. The effective lengths used in experiments ranged from 130 nm to 300 nm (See Figure S2), producing LPR's in the range of 670-970 nm. The nanostructures are asymmetric, allowing for inline second harmonic generation, where the asymmetry ratio used in all experiments was of 0.16-0.2 to maximize nonlinear emission [18]. The samples were also measured for different pitch, 400, 600 and 800 nm, the pitch did not show any significant effect beyond enhanced absorption crossection.

Section S2. Temporal pulse profile as a function of the linear chirp parameter.

In our systematic scans, we observe the generated nonlinear second harmonic (SH) profile as a function of the linear chirp parameter varying from -150 to 150 fs^2, where a 150 fs^2 value corresponds to a stretched pulse of ~ 155 fs FWHM (See Figure S1). As dictated by the Fourier transform, the second order phase coefficient, also known as the linear chirp parameter, corresponds to linearly stretching the pulse. The exact relation can be analytically calculated for a Gaussian pulse. However, generally, the relation between the linear chirp parameter and the duration of the pulse depends on the pulse spectrum and can numerically calculated by a fast Fourier transform (FFT) algorithm:

$$\boldsymbol{E(t) = \int_{-\infty}^{\infty} E_0(\omega) \cdot e^{i\phi(\omega)} e^{-i\omega t}\, d\omega}$$

Where $\boldsymbol{E(t)}$ is the temporal profile of the electric field after pulse shaping, $\boldsymbol{E_0(\omega)}$ is the electric fields spectrum before pulse shaping. The SLM is used only a spectral phase mask, meaning that the power spectrum is not changed throughout the experiment, while the electric field's spectral phase is manipulated readily manipulated at will by the pulse shaper SLM. $\phi(\omega)$ is the spectral phase mask applied by the pulse shaper SLM. When applying only a linear chirp modulation, the phase function takes the form of $\phi(\omega) = \phi_2 \cdot \omega^2$, where ϕ_2 is the linear chirp parameter that is set by the pulse shaping apparatus. In Figure S1, we provide our simulation results for the temporal intensity profile of our pulse as a function of the linear chirp parameter.

Section S3. Nonlinear optical response for nanostructured nonlinearities via a 3-level model solved to the second order in a time-dependent perturbation framework.

We model the nonlinear dynamics of the photo-excited localized plasmonic resonance based on a resonant three-level system. We ascribe the intermediate level as the LSP frequency, the excited state as the SH excitation frequency and ground state as the relaxed state of the system (see Figure 4). By perturbative expansion, we solve the system up to the second order and obtain the amplitude for excitation

$$\boldsymbol{P^{(2)}(\Omega_{SHG}) \propto \int \frac{E(\omega)\, E(\Omega_{SHG}-\omega)}{\omega-\omega_R+i\Gamma_{int}}\, d\omega}$$

Where $E^{(2)}(\Omega_{SHG})$ is the second order probability amplitude for excitation at frequency Ω_{SHG}, and the predicted SHG is proportional to its absolute value squared. ω_R is the LSP resonant frequency, Γ_{int} is the effective interaction linewidth. $E(\omega) = |E(\omega)| \times e^{i\phi(\omega)}$ is the electric field driving the interaction that is composed of the power spectrum $\big||E(\omega)|\big|$ and is constant throughout the experiment. The spectral phase of the pulse, $\phi(\omega)$, can be controlled via the SLM. We note that in the limit of a highly detuned resonant level, our solution approaches the known instantaneous solution found in the traditional treatment of non-resonant nonlinear optics [40]. As can be seen for the expression for $P^{(2)}(\Omega_{SHG})$ that predicts SHG, the nonlinearity is produced separately for each frequency in the manifold of target second harmonic excitations (for a range of Ω_{SHG}). Hence, predicting the optimal pulse shape $\phi(\omega)$ would fundamentally depend on the choice of the SH excitation frequency Ω_{SHG} that would be eventually maximized, such that $\phi_{optimal} = \phi(\omega, \Omega_{SHG})$. Therefore, obtaining a global maximizing phase function, that maximizes

the excitation for all SH frequencies, requires analysis of a range of frequencies. For the LPR excitation, we calculated and verified by simulation that the phase globally maximizing a specific SH frequency is $\phi_{optimal} = \frac{1}{2}\left(tan^{-1}\left(\frac{\Gamma_{Int}}{\omega-\omega_R}\right) + tan^{-1}\left(\frac{\Gamma_{Int}}{\omega+(\omega_R-\Omega_{SHG})}\right)\right)$.

Obtaining the *global* optimal solution demands paying special attention to the symmetrization stemming from the convolution structure dictated by the nonlinear dynamics. By analyzing our pulse spectrum and the plasmonic properties in our experiments, we obtained and verified experimentally, as well as in our simulations, that the optimal phase globally maximizing SHG for a range of SH frequencies Ω_{SHG} is $tan^{-1}\left(\frac{\Gamma_{atan}}{\omega-\omega_{atan}}\right)$.

Section S3. The pictorial representation in the complex plane, which portrays the accumulative contributions of all spectral components in the interaction.

As described in Section S2, our model is based on a 3 level system interaction, solve to the second order in a time-dependent perturbative expansion, $P^{(2)}(\Omega_{SHG}) \propto \int \frac{E(\omega)\,E(\Omega_{SHG}-\omega)}{\omega-\omega_R+i\Gamma_{int}} d\omega$.

The final amplitude for excitation at frequency Ω_{SHG} is proportional to the absolute value of the complex valued amplitude $\propto \left|P^{(2)}(\Omega_{SHG})\right|$. Rewriting the integral as a Riemannian sum we obtain $\propto \sum_i \frac{E(\omega_i)\,E(\Omega_{SHG}-\omega_i)}{\omega_i-\omega_R+i\Gamma_{int}}$, or more generally: $\propto \sum_i p_i^{(2)}$. where each term can be rearranged to form a vector $\left(real\left(p_i^{(2)}\right), imag\left(p_i^{(2)}\right)\right)$ which is portrayed on the 2D plane. The final excitation amplitude is $P^{(2)}(\Omega_{SHG}) \propto \left|p_1^{(2)} + p_2^{(2)} + p_3^{(2)} \ldots\right| = \left|\left(real\left(p_1^{(2)}\right), imag\left(p_1^{(2)}\right)\right) + \left(real\left(p_2^{(2)}\right), imag\left(p_2^{(2)}\right)\right) + \cdots\right|$. Notice that each vector in the sum has an amplitude (arrow

size) $\left|p_i^{(2)}\right|$ and phase $\theta_i = \mathrm{atan}\left(imag\left(p_i^{(2)}\right), real\left(p_i^{(2)}\right)\right)$. Hence, difference arrows in the sum interfere according to their phase difference (the relative angle between them when placed on the 2D plane). Therefore, each vector (term) represents a pathway (small arrow in Fig 4B) leading to an excitation in a excitation frequency Ω_{SHG}. The absolute value of the sum of pathways is the final trajectory (large arrow). By viewing the trajectory bending in the case of a transform limited pulse which carries no phase, as can Figure 3B or Figure 3C left, it is apparent that the plasmonic excitation has a self-interfering contribution to the interaction. This immediately implies that by adding a complementary phase to the interaction via the electric field, it is possible to elongate the trajectory and obtain a larger final excitation amplitude. To further explain the pictorial picture, we illustrate the second order interaction for a chirped pulse in the case of an instantaneous interaction (see Figure S3). An instantaneous interaction is represented in our model by setting the coherence to be extremely small compared to the pulse length. As in Figure S3, each small arrow consists of the mutual contribution of a frequency pair that sum to Ω_{SHG}. The angle of the arrow, meaning the phase of the pathway, is comprised of both the phase of the pulse and the nanostructure and dependes of the modeling of the interaction. In the case of an instantaneous interaction

$$\boldsymbol{\theta = \phi_2 \cdot \omega_1^2 + \phi_2 \cdot \omega_2^2 - \mathrm{atan}\left(\frac{\Gamma_{int}}{\omega - \omega_R}\right)}$$

Since the coherence time is very small, the inversely proportional interaction linewidth $\boldsymbol{\Gamma_{SHG}}$ is very large, the inverse tangent function can be approximated as a constant global phase that doesn't affect the interaction.

$$\boldsymbol{\rightarrow \theta = \phi_2 \cdot \omega_1^2 + \phi_2 \cdot (\omega_1 - \Omega_{SHG})^2 + constant}$$

Section S4. Symmetrization owing to the convolution structure of a second order process.

In the second order solution to the perturbative expansion for a resonant 3 level excitation, the excitation amplitude has the following form:

$$P^{(2)}(\Omega_{SHG}) \propto \int \frac{E(\omega)\, E(\Omega_{SHG}-\omega)}{\omega-\omega_R+i\Gamma_{int}} d\omega$$

Where Ω_{SHG} is the excited frequency, ω_R is the resonant frequency and Γ_{int} is the effective linewidth for the interaction.

Viewing the electric field in terms of amplitude and phase $E(\omega) = |E(\omega)|e^{i\phi(\omega)}$, a symmetrization of the effective phase contributing to the calculations emerges though the convolutional structure to the calculation. We define the effective phase of the electric field $f_\Omega(\omega)$ as :

$$f_\Omega(\omega) \equiv \phi(\omega) + \phi(\Omega-\omega)$$

We note that $f_\Omega(\omega)$ is symmetric around $\frac{\Omega}{2}$:

$$f_\Omega\left(\frac{\Omega}{2}+\delta\right) = \phi\left(\frac{\Omega}{2}+\delta\right) + \phi\left(\Omega-\frac{\Omega}{2}-\delta\right) = \phi\left(\frac{\Omega}{2}+\delta\right) + \phi\left(\frac{\Omega}{2}-\delta\right) = f_\Omega\left(\frac{\Omega}{2}-\delta\right)$$

Therefore, any asymmetry around the target frequency in ϕ would be removed by the symmetrization and will not contribute to the coherent accumulation in the interaction. In addition, since the interaction simultaneously occurs for a range of target frequencies, the symmetrization structure effectively enables to impose phases which are manifested differently for each excitation frequency. Importantly, this restriction must be taken into consideration when calculating the optimal pulse shape for a range of frequencies.

Section S5. The nanostructure induces self-interfering pathways to the overall excitation.

In the second order solution to the perturbative expansion for a resonant 3 level excitation, the excitation amplitude has the following form:

$$\propto \int \frac{E(\Omega-\omega)E(\omega)}{\omega-\omega_R+i\Gamma_{NS}}d\omega$$

Therefore, rearranging the weight function which stems from the localized plasmonic interaction in terms of amplitude and phase results in:

$$\frac{1}{\omega-\omega_R+i\Gamma_{NS}}=\left|\frac{1}{\omega-\omega_R+i\Gamma_{NS}}\right|e^{iatan(\Gamma_{NS},\omega-\omega_R)}$$

Meaning that the nanostructure contributes in an inherent phase function which intrinsically interferes destructively in the interaction process.

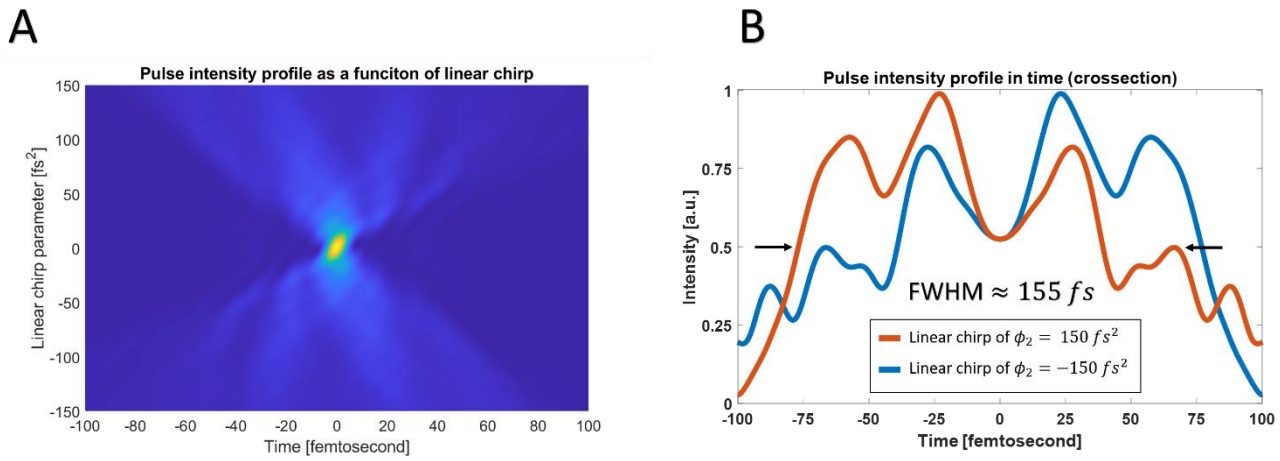

Figure S1 Pulse intensity profile. (A) The pulse intensity profile simulated as a function of the linear chirp parameter, as dictated by the Fourier transform (B) cross-sections from (A) showing the pulse intensity profile from linear chirp of 150 and -150 $\boldsymbol{fs^2}$. The pulse full width at half maximum is approximately 155 femtoseconds.

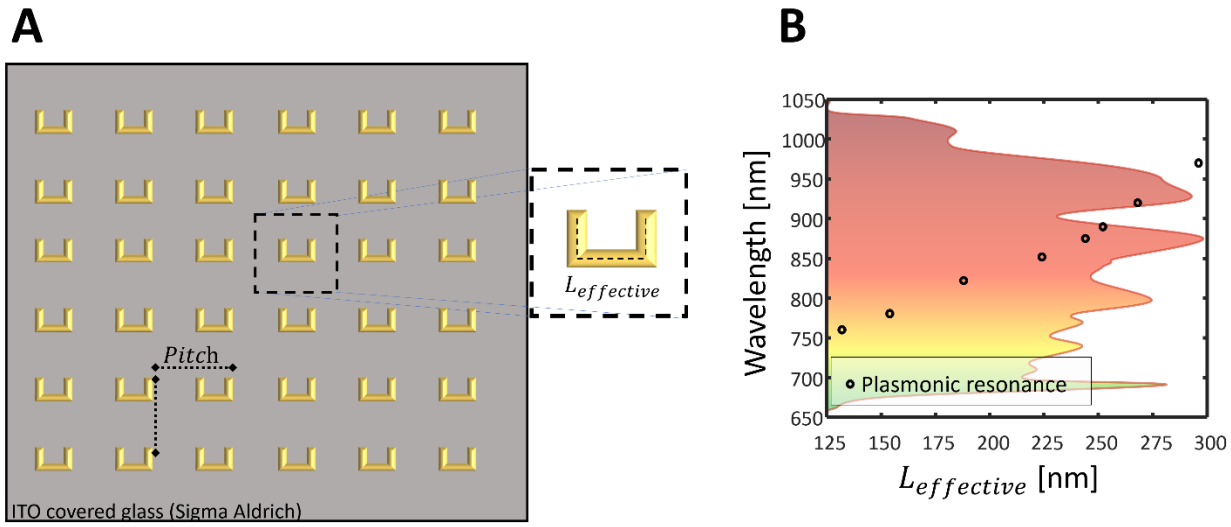

Figure S2 A) Illustration of a sample containing plasmonic nanostructures. Each sample is a 50 by 50 micrometer array containing nanostructures sharing their effective length. The effective lengths used in experiment range in 130 – 300 nm, producing LPR's in the range of 770 - 970 nm. The pitch in both axes was set to be equal and ranged in 500, 700 and 800 showing no significant pitch–related effects in the pulse shaping experiments **B)** Measurements of the nanostructures localized plasmonic resonance as a function of effective length. The lasers spectrum is superimposed, in logarithmic scale, showing the relative locations of the nanostructures resonance in relation to the lasers spectra.

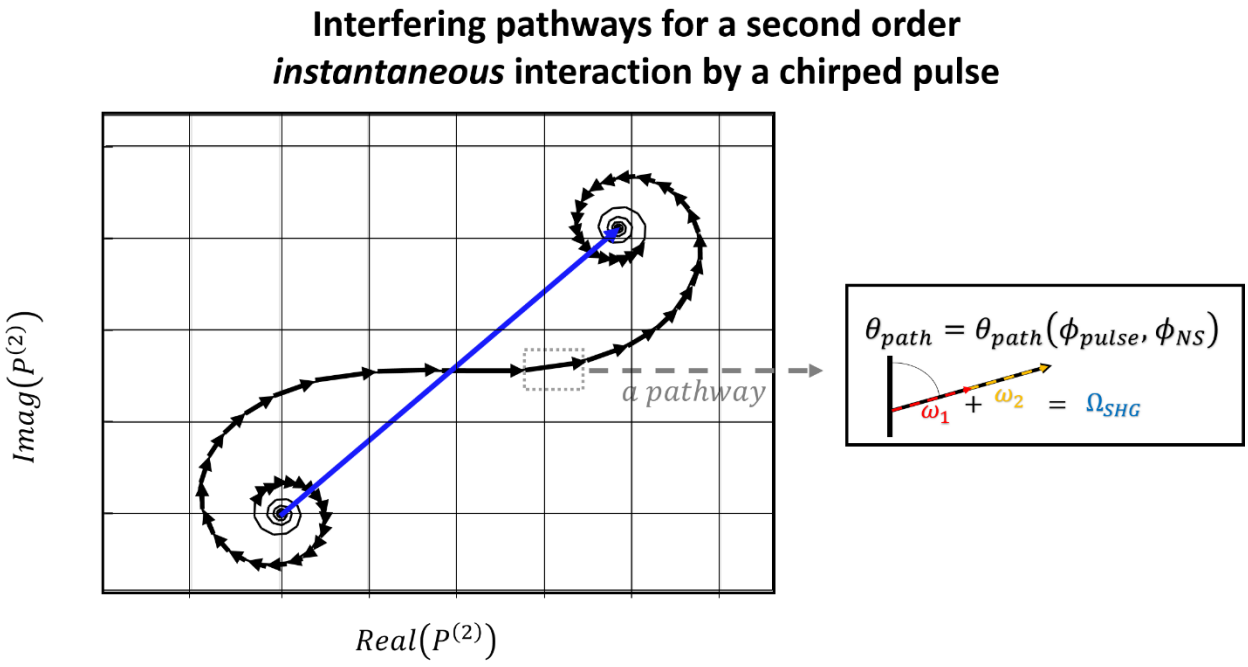

Figure 3S Interaction trajectory for an instantaneous interaction with a stretched pulse. If the coherence time of the interaction is very short relative to the pulse the interaction is effectively instantaneous. In such a case the interfering pathways reflect the pulses phase contribution which results, in the case of a linear chirp, in an Euler spiral. Each small arrow in the trajectory represents an interaction pathway leading the second order excitation at frequency $\boldsymbol{\Omega_{SHG}}$ and is comprised of the amplitude contribution of both frequencies as well as the phase contribution by both frequencies and the nanostructure response. The final excitation is proportional to the final amplitude that is represented by the large blue arrow.